Journal of Chromatographic Science 2013;51:273–285
doi:10.1093/chromsci/bms138 Advance Access publication September 13, 2012

Article

Chemical Profiling of the Chinese Herb Formula Xiao-Cheng-Qi Decoction Using Liquid Chromatography Coupled with Electrospray Ionization Mass Spectrometry

Hai-Yu Zhao[1†], Miao-Xuan Fan[1,2†], Xu Wu[1], Hong-Jie Wang[1], Jian Yang[1], Nan Si[1] and Bao-Lin Bian[1*]

[1]Institute of Chinese Materia Medica, China Academy of Chinese Medical Sciences, Beijing 100700, China, and [2]Beijing Institute for Drug Control

*Author to whom correspondence should be addressed. Email: bianbaolin9@yahoo.com.cn
†These authors contribute equally to this paper.

Received 27 February 2012; revised 15 June 2012

An approach was established to analyze the chemical profiling of Xiao-Cheng-Qi Decoction (XCQD) using liquid chromatography coupled with electrospray ionization tandem mass spectrometry. XCQD consisted of three herbal medicines (*Rhubarb*, *Fructus Aurantii Immaturus* and *Cortex Magnoliae Officinalis*). The traditional water extractive method was applied in the sample preparation, which was identical with clinical use. The characteristic fragmentation pathways of 17 reference compounds were comprehensively studied, including precursors of tannins, flavonones, anthraquinones and lignan. In total, 71 constituents were identified or tentatively characterized based on their mass spectrometry fragmentations and chromatographic behaviors. By comparing their relative contents, flavanones and anthraquinones were supposed to be used together for the quality control of XCQD. Further pharmacology and pharmacokinetics investigations should be performed on the basis of the present chemical profiling study.

Introduction

Xiao-Cheng-Qi Decoction (XCQD) is a classical Chinese herb formula that originated from Shang Han Lun in approximately 200 AD. Currently, it is still attracting interest because of its clinical uses for treating chronic constipation, food stagnation, hypertension, epilepsy, hepatic injury and difficulty in urination (1, 2). All of these clinical effects have been proven during long-term clinical practices. XCQD consists of *Rhubarb* (Da-Huang), *Fructus Aurantii Immaturus* (Zhi-Shi) and *Cortex Magnoliae Officinalis* (Hou-Po). These constituents contribute various synergistic effects in prescriptions. As the major medicine (monarch medicine), rhubarb provides bidirectional regulation of large intestinal motility in decoctions (3). Additionally, *Fructus Aurantii Immaturus* and *Cortex Magnoliae Officinalis* prevents rhubarb-induced disturbances of the regular spiking activity of colonic circular muscle (4). Additionally, a recent study showed that XCQD possesses vascular permeability reduction, inflammation prevention, hepatic-protection, anti-obesity and lipid-lowering activities (5–7). XCQD also prevents the effects of uraemia and stroke (8, 9). A high-performance liquid chromatography (HPLC) method has been established for the determination of eight compounds in XCQD (10). In the authors' previous study, the major compounds were isolated from the water extract of XCQD, and its volatile oil was analyzed by gas chromatography–mass spectrometry (GC–MS) (11). However, no reports have focused on the chemical profiling of XCQD, which has limited its applications in clinical use. Thus, the performance of a systematic chemical investigation of XCQD is very important and urgent. An online analytical method that avoids time-consuming isolation and provides quick, full-scale elucidation of chemical profiling is essential.

In recent years, MS combined with HPLC has provided a powerful approach for the efficient separation and structural characterization of herbal medicines and natural products (12). Although the HPLC–MS analyses have been made of single *Rhubarb* (Da-Huang) and *Fructus Aurantii Immaturus* (Zhi-Shi) (13, 14), XCQD presents a profile with more complicated constituents profile. As the continuation of the authors' research on the phytochemical analysis of XCQD, reported here is the comprehensive analysis of tannins, flavonones, anthraquinones and lignan in XCQD water extract. The preparation of the sample was in accordance with clinical methods, including the processing of medicines, the ratio of the material drugs, the extraction time and the water dosage. In total, 71 compounds were identified or tentatively characterized based on their mass spectra and chromatography behavior. Seventeen compounds were unambiguously identified by a comparison with the reference standards. In addition, the characteristic electrospray (ESI)-MS fragmentation patterns of the major flavonone glycosides in XCQD were carefully investigated, and their diagnostic fragments were reported.

Experimental

Instrumentation and chromatographic conditions

The analyses were performed on an Agilent series 1100 HPLC (Agilent, Waldbronn, Germany) equipped with a quaternary pump, a diode-array detector (DAD), an auto sampler and a column compartment. The samples were separated on a Zorbax SB-C18 column (250 × 4.6 mm i.d., 5 μm, Agilent) with the column temperature at 30°C. The mobile phase consisted of MeOH (solvent A) and water containing 0.5% acetic acid (solvent B). The gradient program was used as follows: initial 0–15 min, linear change from A–B (10:90, v/v) to A–B (17:83, v/v); 15–20 min, linear change to A–B (30:70, v/v); 20–40 min, linear change to A–B (40:60, v/v); 40–55 min, held for A–B (40:60, v/v); 55–65 min, linear change to A–B (45:55, v/v); 65–90 min, linear change to A–B (70:30, v/v); 90–100 min, linear change to A–B (100:0, v/v). The DAD was monitored at 260 nm, and the online ultraviolet (UV) spectra were recorded in the range of 190–400 nm.

LC–MS experiments were performed using a Finnigan LCQ Advantage ion trap mass spectrometer (Thermo Finnigan, San

Jose, CA), which was connected to the Agilent 1100 HPLC instrument via an ESI source in a split ration of 3:1. Ultrahigh-purity helium (He) was used as the collision gas and high-purity nitrogen (N_2) as the nebulizing gas. The optimized mass spectrometry detector parameters in the negative ion mode were as follows: ion spray voltage, 4.5 kV; sheath gas (N_2), 60 arbitrary units; auxiliary gas (N_2), 15 units; capillary temperature, 340°C; capillary voltage, −20 V; tube lens offset voltage, −10 V. For full scan MS analysis, the spectra were recorded in the range m/z 120–1500. In the data-dependent program, the most two abundant ions in each scan were selected and subjected to tandem mass spectrometry (MS^n, $n = 2–5$). The collision-induced dissociation (CID) energy for MS^n was adjusted to 25% in LC–MS analysis. Meanwhile, the isolation width of precursor ions was 3.0 mass units.

Reference compounds and solvents

Seventeen reference compounds were applied in the ESI-MS analysis, including gallic acid, catechin, trans-cinnamic acid, hesperetin, naringenin, hesperidin, neohesperidin, naringin, aloe-emodin, rhein, emodin, chrysophanol, physcion, 2-carboxy-3,8-dihydroxy-1-methylanthraquinone, emodin-8-O-glucoside, sennoside B and magnolol (Figure 1). Their structures were unambiguously identified on the basis of their spectral data, and purities were approximately 95%, as determined by HPLC analysis. HPLC-grade MeOH (Fisher, Fair Lawn, NJ) was used for HPLC analysis. Deionized water was purified by a Milli-Q system (Millipore, Bedford, MA).

Materials and sample preparation

Seven batches of Da-Huang, Zhi-Shi and Hou-Po were purchased from Beijing Medicinal Materials Company (four batches) and Beijing Renwei Material Chinese Medicine, Ltd. (three batches), which were identified as the radix and rhizoma of *Rheum palmatum*, immature fruit of *Citrus sinensis* and the bark of *Magnolia officinalis*, respectively by Prof. Xi-Rong He (Institute of Chinese Materia Medica, China Academy of Chinese Medical Sciences). Voucher specimens (numbered XCQD S1, S2, S3, S4, S5, S6 and S7) were deposited in the Institute of Chinese Materia Medica, China Academy of Chinese Medical Sciences.

Da-Huang (rice wine processed), Zhi-Shi and Hou-Po (4:3:2), 4.5 g each, were soaked in 45 mL of deionized water for one-half hour and reflux-extracted for 40 min. The solution was filtered through 0.45 μm membranes before use, and a 5 μL aliquot was injected into HPLC for analysis.

Results and Discussion

Altogether, 71 compounds were identified or tentatively characterized in the present study. The general chemical profile of XCQD was clarified (Figure 2). The ESI-MS behavior of 17

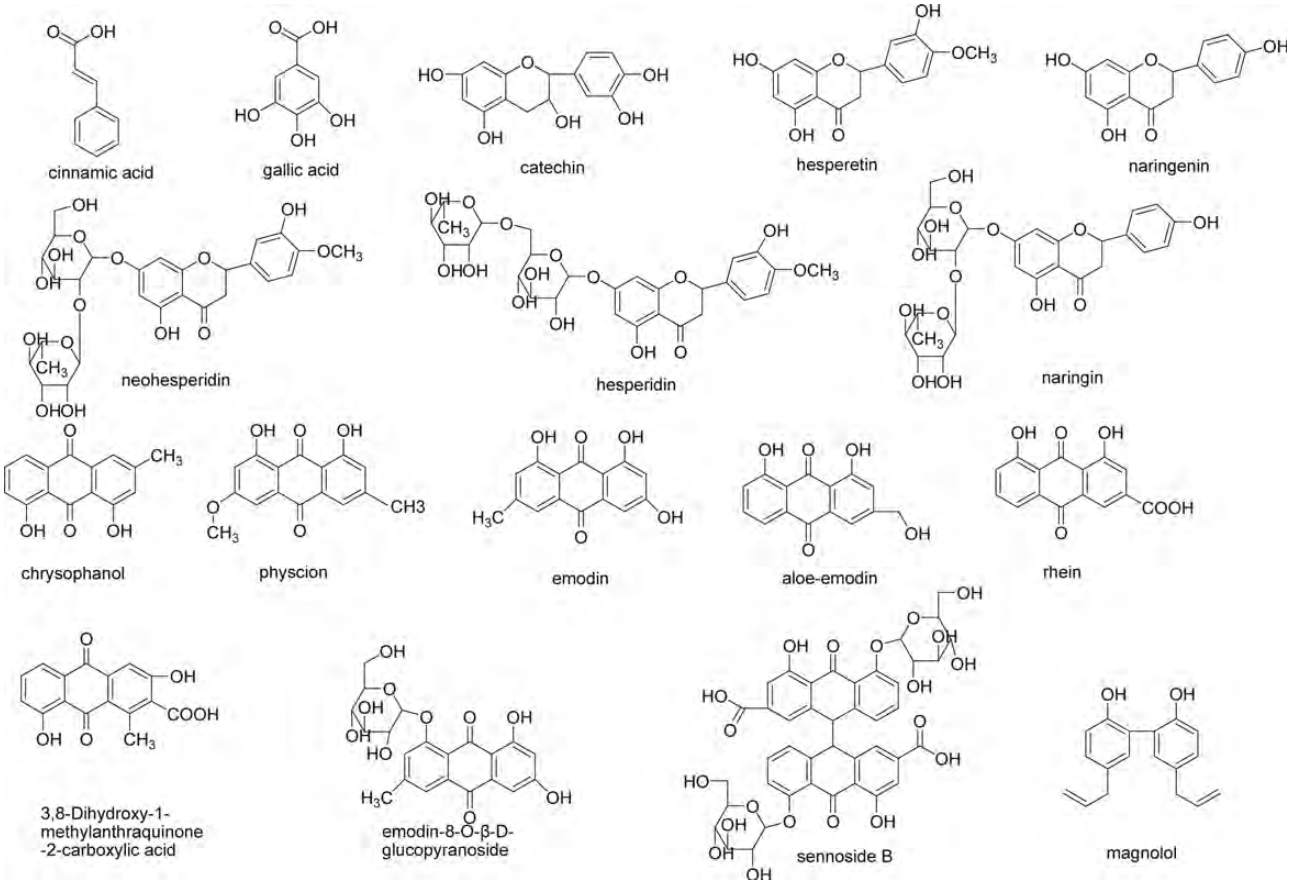

Figure 1. Structures of reference compounds in HPLC–MS^n analysis.

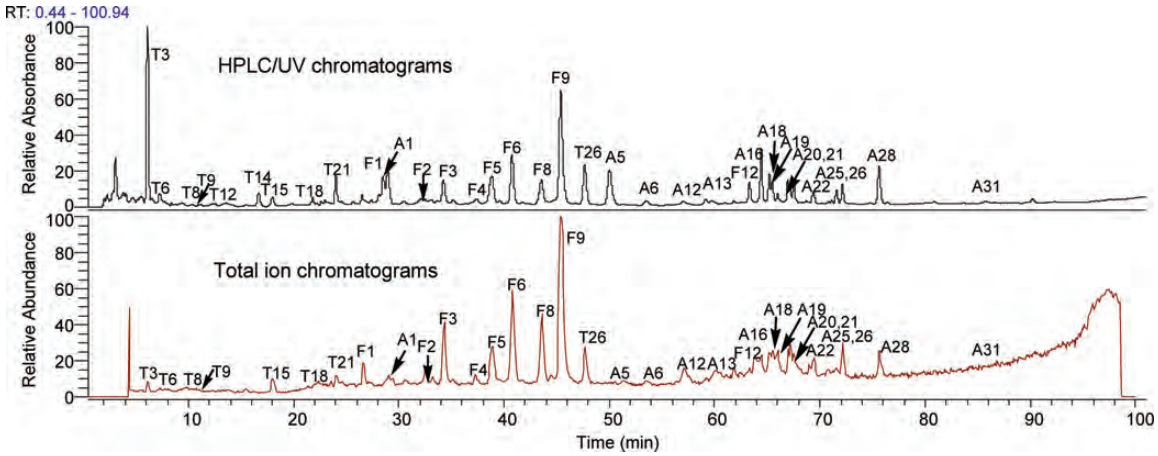

Figure 2. HPLC–UV chromatogram (260 nm) and total ion chromatogram of Xiao-Cheng-Qi Decoction.

reference compounds were comprehensively investigated, including three precursors of tannins, five flavonones, eight anthraquinones and one lignan. All compounds could be detected in HPLC–MS-MS analysis of the XCQD sample, except for cinnamic acid.

Fingerprint similarity analysis of XCQD

The fingerprint similarity of seven batches of XCQD was analyzed by computer aided similarity evaluation (CASE) under UV conditions. The resolutions, areas and heights of the 20 common peaks in HPLC–UV chromatography were considered. The similarity of each batch was more than 0.8 (Table I). The optimization of the column, detected wavelength, pH value of the mobile phase and gradient elution program was performed to achieve the best resolution of peaks. The relative standard deviations (RSDs) of precision, stability and repeatability were individually detected at 0.42, 0.49 and 1.10%.

ESI–MS-MS analysis of gallic acid, catechin and cinnamic acid

Gallic acid, catechin and cinnamic acid and related derivatives originated form rhubarb. As the precursor of tannin, gallic acid presented an $[M\text{-}H]^-$ ion at m/z 169 in the full scan mass spectrum. The fragment of the $[M\text{-}H\text{-}CO_2]^-$ ion at m/z 125 was shown in the MS–MS experiment. This obtained ion was not more easily cracked in further MS^3 analyses (MS^3: the third stage of multi-stage MS analysis).

Additionally, the fragmentation pathway of catechin (MW = 290) was investigated. Its MS-MS spectrum yielded moderate and predominant fragments at m/z 271 and 245, respectively, from the $[M\text{-}H]^-$ ion, which were caused by the losses of the OH group in ring C and the rearrangement of ring A. Further MS^3 experiments presented an $[M\text{-}H\text{-}CO_2\text{-}C_2H_2O]^-$ ion at m/z 203 from its precursor ion at m/z 245. It was yielded by the cleavage of ring C, which has been proven by a heavy water exchange experiment (15). Additionally, an $[M\text{-}H\text{-}CO_2\text{-}H_2O]^-$ ion at m/z 227 and $[M\text{-}H\text{-}CO_2\text{-}C_3H_6O]^-$ ion at m/z 187 were detected.

The ESI-MS of cinnamic acid revealed an $[M\text{-}H]^-$ ion at m/z 147. Its MS-MS spectrum showed an $[M\text{-}H\text{-}CO_2]^-$ fragment at m/z 103.

Table I
Fingerprint Similarity of Seven Batches of XCQD

	S1	S2	S3	S4	S5	S6	S7
S1	1	0.994	0.994	0.827	0.828	0.892	0.970
S2	0.994	1	0.990	0.847	0.846	0.916	0.980
S3	0.994	0.990	1	0.810	0.808	0.886	0.962
S4	0.827	0.847	0.810	1	0.999	0.965	0.934
S5	0.828	0.846	0.808	0.999	1	0.963	0.934
S6	0.892	0.916	0.886	0.965	0.963	1	0.970
S7	0.970	0.980	0.962	0.934	0.934	0.970	1

Although cinnamic acid was not directly detected in the online analysis, its derivatives were widely found in XCQD. Cinnamic acid was probably generated in the process of isolation (16).

Identification of tannins and their precursors

As one kind of major active constituents, tannins have been reported to possess activities of depressurization, antivirus, anticoagulation and other effects (17). In total, 26 tannins and their precursors were identified in XCQD by LC–MS (Table II). Most of these were derivatives of catechin, gallic acid and cinnamic acid from rhubarb. T1 [MW = 332, retention time (t_R) = 4.64 min], T2 (MW = 332, t_R = 5.66 min) and T5 (MW = 332, t_R = 6.65 min) were three isomers of galloyl-O-glucose, which showed $[M\text{-}H]^-$ ions at m/z 331 in full mass spectra. The common fragments $[M\text{-}H\text{-}120Da]^-$, $[M\text{-}H\text{-}glu]^-$ and $[M\text{-}H\text{-}glu\text{-}CO2]^-$ ions were observed in MS-MS spectra. The $[M\text{-}H\text{-}120Da]^-$ ion at m/z 211 was the characteristic loss of glucosyl residue. In addition, the fragment $[M\text{-}H\text{-}60Da]^-$ ion at m/z 271 was also found, which was attributed as the cleavage of glucosyl residue. In the MS^3 spectrum of T5, the obtained ion yielded diagnostic ions at 211 and m/z 169 of galloyl. Due to the different linkage position of glucose, the abundances of m/z 271 and 169 ions in these three isomers were different from each other. According to the literature, the linkage position of glucose should be at C1, C3 and C4 of galloyl residue (18–20).

Additionally, two other isomers of galloyl derivatives were detected. Both T6 (MW = 494, t_R = 7.33 min) and T7 (MW = 494, t_R = 7.86 min) presented $[M\text{-}H\text{-}180Da]^-$ ions at m/z 313 and galloyl fragment at m/z 169 for the parent ion at m/z 493

Table II
HPLC–ESI-MS^n Data Identification of Tannins and their Precursors in XCQD*

Number	Name	T_R (min)	$[M-H]^-$ (m/z)	MS-MS (m/z)
T1	Galloyl-O-glu	4.64	331	MS^2 [331]: 271, 241, 211, **169**, 125 MS^3 [331 → 169]: **125**
T2	Galloyl-O-glu	5.66	331	MS^2 [331]: 271, 211, **169**, 125 MS^3 [331 → 169]: **125**
T3†	Gallic acid	6.14	169	MS^2 [169]: **125**
T4	3, 4-Dihydroxybenzoic acid-O-glu	6.49	315	MS^2 [315]: 233, **153**, 152, 146, 109, 108 MS^3 [315 → 153]: 109, **108**
T5	Galloyl-O-glu	6.65	331	MS^2 [331]: **271** MS^3 [331 → 271]: **211**, 169 MS^4 [331 → 271 → 211]: **168**, 167, 149 MS^5 [331 → 271 → 211 → 168]: **125**
T6	Caffeoyl-O-glu-galloyl	7.33	493	MS^2 [493]: 331, **313**, 283, 271, 241, 169 MS^3 [493 → 313]: 283, 191, 179, **169**, 125, 97
T7	Caffeoyl-O-glu-galloyl	7.86	493	MS^2 [493]: **313**, 169 MS^3 [493 → 313]: 283, 241, 223, **169**, 168, 162, 125 MS^4 [493 → 313 → 169]: **125**
T8	Catechin-O-glu	11.10	451	MS^2 [451]: **289**, 245 MS^3 [451 → 289]: 247, **245**, 231, 218, 205, 137 MS^4 [451 → 289 → 245]: **203**
T9	1-O-Galloyl-(2-O-acetyl)-glu	12.59	373	MS^2 [373]: 331, 313, **169**, 125 MS^3 [373 → 169]: **125**
T10	Caffeoyl-dihydroxy benzoic acid-O-rha	12.88	461	MS^2 [461]: **315**, 135 MS^3 [461 → 315]: 149, **135**
T11	Dimer catechin/epicatechin	13.78	577	MS^2 [577]: 451, **425**, 407, 289 MS^3 [577 → 425]: **407** MS^4 [577 → 425 → 407]: 298, 297, **285**, 283, 282, 257, 255, 243 MS^5 [577 → 425 → 407 → 285]: **257**
T12	Catechin-O-glu	14.22	451	MS^2 [451]: **289**, 245, 161, 147 MS^3 [451 → 289]: 245, 231, 205, 204, 203, 179
T13	Dimmer catechin/epicatechin	15.53	577	MS^2 [577]: 559, 451, **425**, 407, 289, 273 MS^3 [577 → 425]: **407**, 273 MS^4 [577 → 425 → 407]: 389, 363, 297, **285**, 283, 281, 255, MS^5 [577 → 425 → 407 → 285]: **257**, 145
T14	Catechin-O-glu	16.28	451	MS^2 [451]: 307, **289** MS^3 [451 → 289]: **245**, 205, 179, 161 MS^4 [451 → 289 → 245]: **109**
T15†	Catechin	17.59	289	MS^2 [289]: 271, **245**, 205, 203, 179 MS^3 [289 → 245]: 227, **203**, 187, 175, 161 MS^4 [289 → 245 → 203]: **175**
T16	Catechin-O-glucose-malonate	20.70	537	MS^2 [537]: **493** MS^3 [537 → 493]: 451, **289**, 245 MS^4 [537 → 493 → 289]: 245, 230, **205**
T17	Catechin-O-glucose-malonate	21.31	537	MS^2 [537]: **493**, 451, 289 MS^3 [537 → 493]: 451, **289** MS^4 [537 → 493 → 289]: **245**, 209, 205, 203, 175, 167
T18	Dimmer catechin/epicatechin	22.20	577	MS^2 [577]: 559, 451, **425**, 407, 289 MS^3 [577 → 425]: **407** MS^4 [577 → 425 → 407]: 389, 297, 293, **285**, 281, 256, 239, MS^5 [577 → 425 → 407 → 285]: **257**
T19	Catechin-O-glu(OAc)	22.87	493	MS^2 [493]: 475, 455, 448, 298, **289**, 245 MS^3 [493 → 289]: **245**, 231, 206, 188 MS^4 [493 → 289 → 245]: **161**
T20	Dimmer catechin-O-gallolyl	23.85	729	MS^2 [729]: **577**, 559, 451, 425, 407 MS^3 [729 → 577]: 559, 451, 425, **407**, 289 MS^4 [729 → 577 → 407]: **284**, 269
T21	Epicatechin	24.57	289	MS^2 [289]: **245**, 205, 203, 179 MS^3 [289 → 245]: 227, 217, **203**, 188, 187, 161
T22	Catechin-O-galloyl	30.48	441	MS^2 [441]: 331, **289**, 169 MS^3 [451 → 289]:**245**, 205, 203, 175 MS^4 [451 → 289 → 245]: **161**
T23	Hydroxycinnamic acid-gallic acyl-O-glu	30.71	477	MS^2 [477]: **313**, 169 MS^3 [477 → 313]: 223, **169**
T24	Cinnamoyl-O-glu-glu-O-galloyl	41.34	623	MS^2 [623]: **475**, 461, 313 MS^3 [623 → 475]: 457, 331, **313**, 169 MS^4 [623 → 475 → 313]: 169, **151**
T25	Cinnamoyl-glucose-O-galloyl	47.68	461	MS^2 [461]: **313** MS^3 [461 → 313]: **169**, 151, 125 MS^4 [461 → 313 → 169]: **125**
T26	Cinnamoyl-glucose-O-galloyl	53.55	461	MS^2 [461]: 313, 253, 211, **169** MS^3 [461 → 169]: **125**

*Note: Bold characters indicate the base peaks in MS^n spectra.
†Structures confirmed by comparison with reference standards.

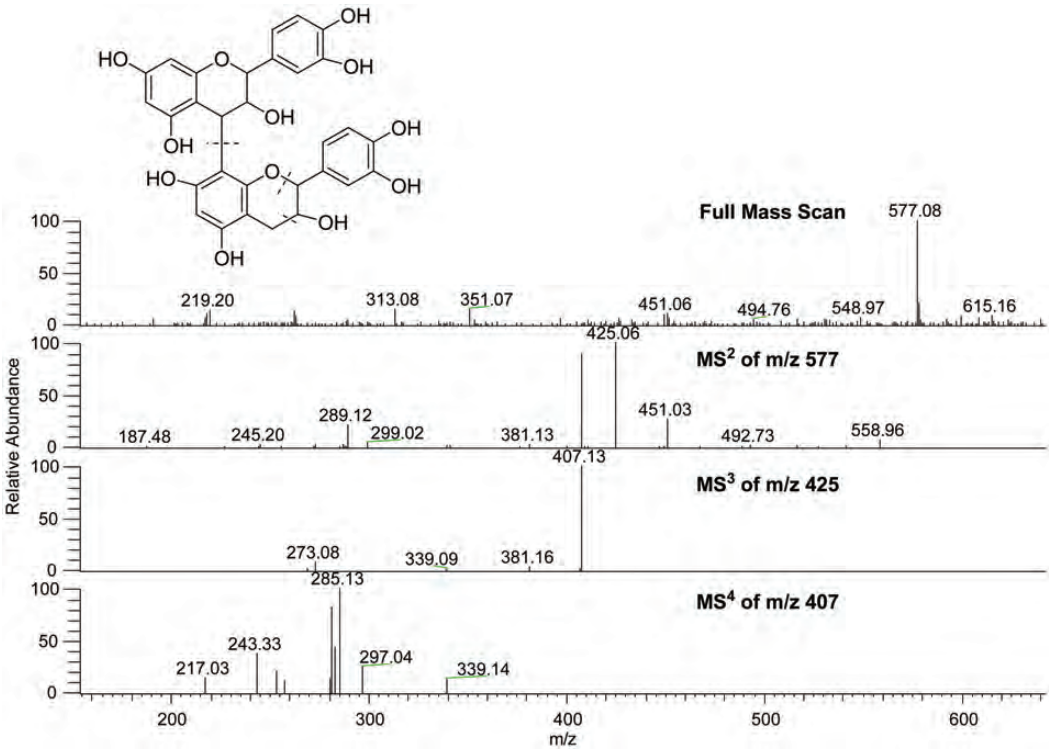

Figure 3. ESI-MS^n spectra for T13, the dimer of catechin/epicatechin.

in their MS–MS spectra. According to the literature, the neutral loss of 180 Da fragment should be deduced as caffeoyl (3,4-dihydroxy-cinnamic acid) (13). In the MS^3 experiment of the $[M\text{-}H\text{-}180Da]^-$ ion, m/z 169 was observed as the base peak. Caffeoyl and galloyl should attach separately at the different positions of glucose. Thus, T6 and T7 were identified as caffeoyl-O-glucose-galloyl (21–23).

T9 (MW = 374, t_R = 12.59 min) was identified as galloyl-O-glu(OAc) because of the characteristic acetylase glucoside loss of 204 Da from the galloyl group. The galloyl residue at m/z 169 was detected as the base peak. T9 was assigned as 1-O-galloyl-(2-O-acetyl)-glucose (24).

Additionally, 13 catechin derivatives were detected in XCQD. Catechin (T15, MW = 290, t_R = 17.59 min) was identified by comparison with the reference. Its isomer T21 at t_R = 24.57 min was deduced as epicatechin based on their identical ESI-MS behavior and eluting order in the chromatogram (25). Three catechin dipolymers (T11, T13 and T18; MW = 578) were observed at t_R = 13.78, 15.53 and 22.20 min, respectively. Their molecular weights were of accord with the formula MW = 290 + (n−1) × 288 (15). All showed similar fragmentation patterns in their MS^n spectra. The $[M\text{-}H\text{-}C_8H_8O_3]^-$ ion at m/z 425 was the base peak in their MS-MS spectra, which was attributed as the Retro Diels-Alder (RDA) reaction of ring C. Meanwhile, the $[M\text{-}H\text{-}H_2O]^-$ ion at m/z 559 and catechin fragment at m/z 289 were clear. Further MS^3 experiments revealed an $[M\text{-}H\text{-}C_8H_8O_3\text{-}H_2O]^-$ fragment at m/z 407 for the parent ion at m/z 425. In the MS^4 spectra (MS^4: the fourth stage of multi-stage MS analysis), this obtained ion yielded an m/z 285 fragment, which was attributed as RDA cracking in the other catechin. The further loss of CO at m/z 257 could be detected in the MS^5 experiment of m/z 285 (Figure 3) (MS^5: the fifth stage of multi-stage MS analysis). Generally, catechin always attached to each other at the 4 → 8 position, forming dipolymers. T11, T13 and T18 were regarded as dipolymers of catechin or epicatechin, which could not be discriminated by using their MS^n spectra.

Meanwhile, a catechin dipolymer adducted with galloyl was detected at 23.85 min (T20, MW = 730). Its MS-MS spectrum yielded a catechin dipolymer ion at m/z 577. The neutral loss of 152 Da was deduced as the fragment of galloyl acid residue. In the following MS^3 experiment, the MS behavior of m/z 577 was the same with the dipolymers of catechin/epicatechin (T11, T13 and T18). The characteristic ions due to the continuous RDA cracking, the loss of H_2O and catechin were observed. Tripolymers and tetramers of catechin, which could be found in rhubarb, were not detected in XCQD (17). This may be because of the hydrolysis in the decoction process.

Furthermore, three catechin-O-glucose isomers (T8, T12 and T14) were identified at 11.10, 14.22 and 16.28 min. All yielded $[M\text{-}H\text{-}162Da]^-$ ions at m/z 289 in MS-MS spectra. The obtained aglycone ion generated a special $[M\text{-}H\text{-}CO_2]^-$ ion at m/z 245, which was identical to catechin. In addition, catechin-O-glu(OAc) was found at 22.87 min (T19, MW = 494) due to the loss of 204 Da in its MS-MS spectrum (26).

Additionally, T16 (MW = 538, t_R = 20.70 min) and T17 (MW = 538, t_R = 21.37 min) were detected as another type of catechin glycosides. In their MS-MS spectra, the first loss of 44 Da indicated the cleavage of COOH. Further MS^3 spectra revealed the loss of 204 Da and yielded a catechin ion at m/z 289. All of this information supported the existence of glucose-malonate. The gradual neutral loss of 44 Da and 204 Da were

considered to be the characteristic MS fragmentation of glucose-malonate, which has been comprehensively reported in rhubarb (27). Thus, T16 and T17 were deduced to be two isomers of catechin-O-glucose-malonate.

Apart from these, T25 (MW = 462, t_R = 47.68 min) and T26 (MW = 462, t_R = 53.35 min) presented $[M-H]^-$ ions at m/z 461 in full scan mass spectra. The neutral loss of 148 Da at m/z 313 in their MS-MS spectra indicated the substitution of cinnamoyl. Further MS^3 spectra gave an $[M-H\text{-cinnamoyl-glu}]^-$ ion at m/z 169. This obtained ion produced a characteristic ion of galloyl at m/z 125. Thus, T25 and T26 were identified as a couple of isomers of cinnamoyl-O-glucose-O-galloyl (20, 28). Additionally, the cinnamoyl-O-glucose-glucose-O-galloyl (T24, MW = 624, t_R = 41.34 min) was detected, which presented one more sugar than T25 and T26.

ESI–MS-MS analysis of flavonones

ESI-MS-MS analysis of five flavonones was performed, including naringenin, naringin, hesperetin, hesperidin and neohesperidin.

In the negative ion model, naringenin gave an $[M-H]^-$ ion at m/z 271 in full scan mass spectrum. Due to the RDA reaction at ring C, its MS-MS spectrum showed the base peak at m/z 151. The special moderate ion caused by the loss of ring B at m/z 177 was also found. In the low molecular weight range, the fragments at m/z 119 and 93 were attributed as the collision fragments of ring B (29).

Naringin (naringenin-7-O-neohesperidose) revealed a different fragmentation pattern from naringenin. The frequent collision of neohesperidose yielded an $[M-H-120Da]^-$ ion at m/z 459 and an $[M-H-rha-120Da]^-$ ion at m/z 313 in the MS-MS spectrum. Among them, m/z 459 was shown as the base peak. The $[M-H-rha]^-$ ion at m/z 433 was also observed, but it was not obvious. In the MS^3 experiment of aglycone ion at m/z 271, the $[M-H-rha-glu-60Da]^-$ fragment at m/z 211 was found as the base peak, which was totally different from that of naringenin (Figure 4). However, the aglycone fragmentation of naringenin-4′-O-glycosides was almost the same as naringenin (30). This was atrtributable to the acidity difference of 7-OH and 4′-OH.

Hesperidin (hesperetin-7-O-glu-1,6-rha) and neohesperidin (hesperetin-7-O-glu-1,2-rha) were also investigated in this study. The structure difference between these two isomers only existed in the attached position of outer rhamnose at the C-7 position. Apart from the aglycone ion at m/z 301, a series of $[M-H-120Da]^-$, $[M-H-rha-120Da]^-$ and $[M-H-rha-glu]^-$ ions was observed in the MS^2 spectrum of neohesperidin (MS^2: the second stage of multi-stage MS analysis). However, in the MS^2 analysis of hesperidin, only the $[M-H-rha-glu]^-$ ion at m/z 301 was found. Thus, $[M-H-120Da]^-$ and $[M-H-rha-120Da]^-$ ions seemed to be the characteristic ions of flavanone 7-O-neohesperidose glycoside (Figure 5).

Identification of flavanones

According to the ESI-MS analysis of five reference compounds, 13 flavanones were detected in XCQD (Table III). These types of flavanones were from *Fructus Aurantii Immaturus*.

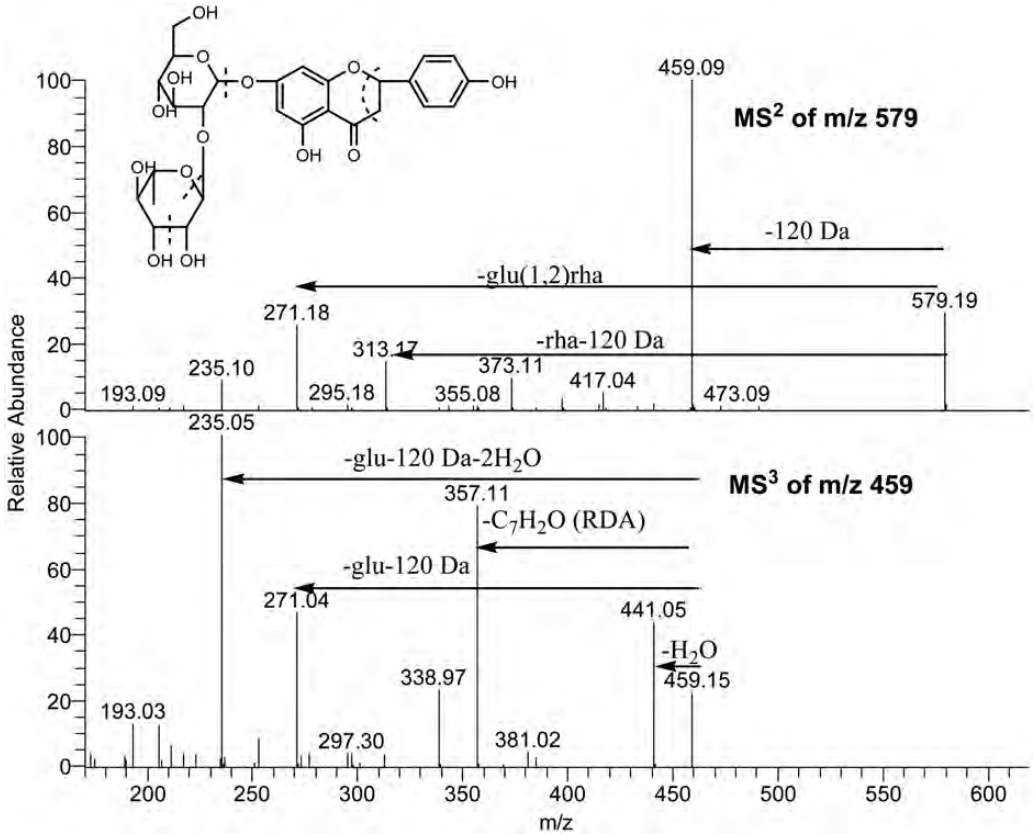

Figure 4. ESI-MS^n spectra for naringin.

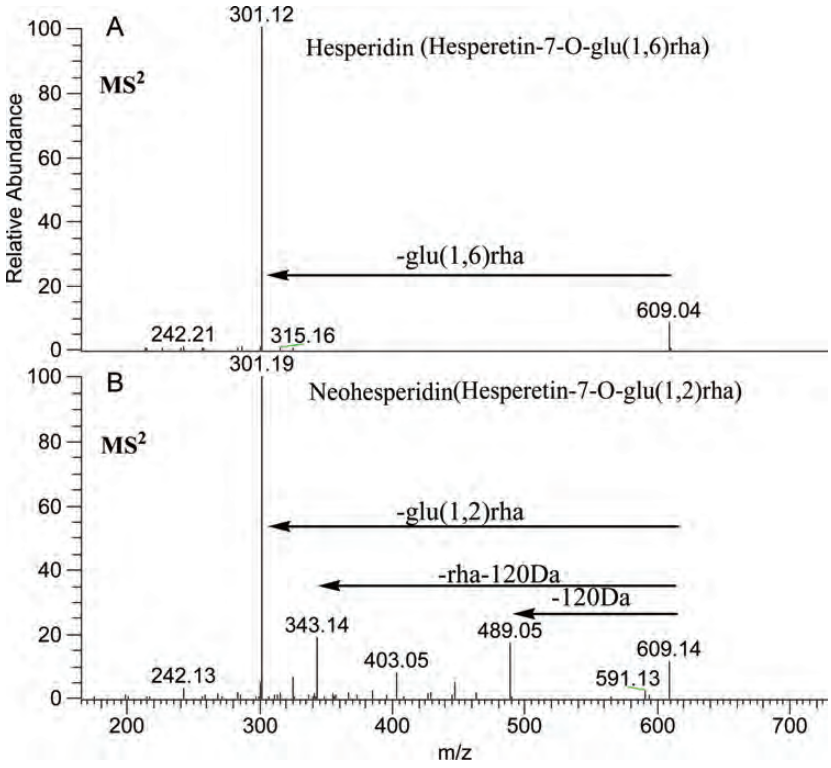

Figure 5. ESI-MS^2 spectra: hesperidin (A); neohesperidin (B).

F1 (MW = 758, t_R = 27.92 min) first presented an $[M\text{-}H]^-$ ion at m/z 757. Its MS-MS spectrum gave the base peak at m/z 449, indicating the loss of glucose and rhamnose. The moderate peak at m/z 595 was attributed to be the rupture of glucose from the other position of aglycone. Meanwhile, the aglycone ion was shown to be the base peak at m/z 287 in the MS^3 spectrum, which was attributed as OH-naringenin. Additionally, RDA clicking yielded a fragment at m/z 151 in the further MS^4 spectrum. Compared with naringenin, the linkage of additional OH should be on ring B. Thus, this aglycone was deduced as eriodictyol (4′-OH-naringenin). According to the abundance of diagnostic ions, two sugar chains should attach at C7 and C4′, respectively. Therefore, F1 was tentatively identified as eriodictyol-4′-O-glu-7-O-glu-1,6-rha (31).

With the same aglycone as F1, F2 (MW = 596, t_R = 32.43 min) and F3 (MW = 596, t_R = 34.25 min) were observed as a pair of eriodictyol-glycoside isomers. In the MS-MS spectrum of F2, the loss of rutinoside yielded a base peak at m/z 287. The characteristic ion at m/z 151 was found in a further MS^3 spectrum. According to the literature, F2 was deduced as eriodictyol-7-O-rutinoside from *Fructus Aurantii Immaturus* (32). As a comparison, F3 presented a predominant $[M\text{-}H\text{-}OH\text{-}120Da]^-$ ion at m/z 459 in the MS-MS spectrum, indicating the existence of neohesperidose (glu-1,2-rha). The aglycone ion at m/z 287 was also observed. In the further MS^3 experiment of m/z 459, fragments at m/z 441, 357 and 235 were detected. Thus, F3 was tentatively identified as eriodictyol-7-O-neohesperidose (33, 34). This conclusion was also supported by the elution order (glu-1,2-rha eluted faster than glu-1,6-rha) of F2 and F3, which depended on their polarity difference.

As a flavonone glycoside with three sugars, F4 was observed at t_R = 37.25 min with $[M\text{-}H]^-$ ion at m/z 771. Its MS-MS spectrum revealed an aglycone ion at m/z 301 as the base peak. The loss of sugar residues ions at m/z 609, 489 and 343 were detected with low abundances. According to their abundance patterns, three sugars were deduced as one substitution chain on the aglycone (35). The existence of an $[M\text{-}H\text{-}glu]^-$ ion at m/z 609 and an $[M\text{-}H\text{-}glu\text{-}120Da\text{-}rha]^-$ ion at m/z 343 indicated that rhamnose and one glucoses were attached on the other sugar. In the MS^3 of the aglycone ion at m/z 301, the fragments were identical with hesperetin. Therefore, F4 was assigned as hesperitin-7-O-(rha, glu)-glu.

F7 (MW = 756, t_R = 43.60 min) presented an $[M\text{-}H]^-$ ion at m/z 755 in full scan mass spectrum. Its MS-MS spectrum clearly generated the $[M\text{-}H\text{-}rha]^-$ ion at m/z 609 and $[M\text{-}H\text{-}rha\text{-}120Da]^-$ ion at m/z 489, which supported the existence of glu-1,2-rha. Meanwhile, the aglycone ion at m/z 301 was found to be the base peak. The special ions at m/z 286, 242 in the further MS^3 experiment of m/z 301 indicated that its aglycone was hesperetin. In accordance with the literature, F7 was deduced as hesperetin-7-O-(2”,6”-di-O-rha)-glu (36).

By comparison with standards, F8 (MW = 610, t_R = 44.14 min) and F9 (MW = 610, t_R = 45.45 min) were unambiguously identified as hesperidin (hesperetin-7-O-glu-1,2-rha) and neohesperidin (hesperetin-7-O-glu-1,6-rha) (Figure 6).

In addition, naringenin and its derivatives were detected as the other important flavonone aglycones in XCQD. In the extract ion chromatograms (XIC) of m/z 579 (Figure 6), F5

Table III
HPLC–ESI-MS^n Data Identification of Flavonones in XCQD*

Number	Name	T_R (min)	$[M-H]^-$ (m/z)	MS-MS (m/z)
F1	Eriodictyol-4′-O-glu-7-O-glu-1,6-rha	27.92	757	MS^2 [757]: 595, **449**, 287 MS^3 [757 → 449]: **287** MS^4 [757 → 449 → 287]: **151**, 135
F2	Eriodictyol-7-O-rutinoside	32.34	595	MS^2 [595]: **287** MS^3 [595 → 287]: **151** MS^4 [595 → 287 → 151]: **107,** 65
F3	Eriodictyol-7-O-neohesperidose	34.25	595	MS^2 [595]: **459**, 235 MS^3 [595 → 459]: 441, 357, 339, 295, 271, **235**, 211, 205, 203, 193, 151 MS^4 [595 → 459 → 235]: 217, **205**, 191, 179 MS^4 [595 → 459 → 357]: 339, 169, **151**, 150
F4	Hesperitin-7-O-(rha, glu)-glu	37.25	771	MS^2 [771]: 609, 489, 447, 343, **301** MS^3 [771 → 301]: **286**, 283, 257, 242, 228, 199, 164 MS^4 [771 → 301 → 286]: 258, **242**, 240, 227, 215, 199, 185, 125
F5	Isonaringin	38.83	579	MS^2 [579]: **271** MS^3 [579 → 271]:183, 177, 169, 165, **151**, 119, 107 MS^4 [579 → 271 → 151]: **107**
F6†	Naringin	40.84	579	MS^2 [579]: **459**, 441, 433, 313, 271, 235 MS^3 [579 → 459]: 441, **357**, 339, 271, 267, 235, 211, 151 MS^4 [579 → 459 → 357]: 339, **191**, 151
F7	Hesperetin-7-O-(2″,6″-di-O-rha)-glu	43.60	755	MS^2 [755]: 609, 489, 325, **301** MS^3 [755 → 301]: **286**, 283, 258, 257, 242, 227 MS^4 [755 → 301 → 286]: **258**, 242, 216, 215, 177, 174
F8†	Hesperidin	44.14	609	MS^2 [609]: **301** MS^3 [609 → 301]: 286, 283, 258, 257, **242**, 199
F9†	Neohesperidin	45.45	609	MS^2 [609]: 489, 343, **301** MS^3 [609 → 301]: **286**, 283, 268, 258, 257, 242 MS^4 [609 → 301 → 286]: 258, 242, 240, 215, **199**, 198, 174, 161
F10	Dihydroxy-methoxy-flavonone-O-rutinoside	57.80	593	MS^2 [593]: **285** MS^3 [593 → 285]: 270, 267, 255, **243**, 241, 198, 175, 164 MS^4 [593 → 285 → 243]: 229, **215**
F11†	Naringenin	58.72	271	MS^2 [271]: 177, **151**, 119, 107, 93 MS^3 [271 → 151]: **107**
F12†	Hesperetin	62.44	301	MS^2 [301]: **286,** 283, 268, 258, 257, 242, 241, 227, 215, 199, 125 MS^3 [301 → 286]: 268, 258, 257, **242,** 215, 201, 199, 174 MS^4 [301 → 286 → 242]: **199**
F13	Naringenin-7-O-glu(OAc)-1,6-rha	75.01	621	MS^2 [621]: 579, 561, 533, 519, **501**, 483, 459, 417, 339, 271 MS^3 [621 → 501]: 381, 369, **357,** 339, 336, 296, 217, 177, 151 MS^4 [621 → 501 → 357]: 339, 169, **151**

*Note: Bold characters indicate the base peaks in MS^n spectra.
†Structures confirmed by comparison with reference standards.

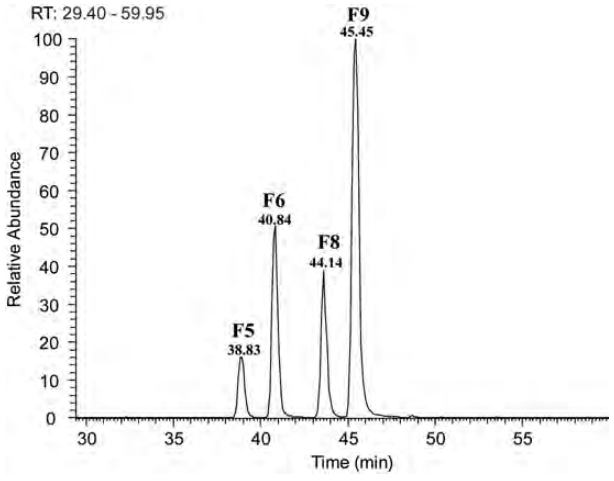

Figure 6. XIC of 579 (F5 and F6) and 609 (F8 and F9).

and F6 were observed at 38.83 and 40.84 min, respectively. F6 was unambiguously identified as naringin (naringenin-7-O-glu-1,2-rha) by comparison with the reference. Its characteristic ion was found at m/z 459 . However, F5 exhibited different ESI-MS. In its MS-MS spectrum, the $[M-H]^-$ ion at m/z 579 yielded the base peak at m/z 271, indicating the aglycone of naringenin. The neutral loss of 308 Da group resulted from the cleavage of the glu-rha group. In terms of the ESI-MS fragmentation analysis of rutinose and neohesperidose, F5 was identified as isonaringin (naringenin-7-O-glu-1,6-rha) (37).

The $[M-H]^-$ ion of F13 at m/z 621 produced an $[M-H-120Da]^-$ ion at m/z 501 as the base peak in its MS-MS spectrum. At the same time, the diagnostic ion at m/z 459 and the aglycone ion at m/z 271 were found. The MS^3 experiment of m/z 501 gave special ions at m/z 357 and 151, which were identical to those of naringin. Thus, F13 was deduced as naringenin-7-O-glu(OAc)-1,6-rha (38).

Additionally, a flavonone glycoside with di-OH-OCH3-flavanon aglycone was observed. F10 was detected at 57.80 min and revealed an $[M-H]^-$ ion at m/z 593. Its MS-MS spectrum yielded a product ion at m/z 285 as the base peak. This obtained aglycone ion produced an $[M-H-glu-rha-CH2]^-$ ion at m/z 270 and an $[M-H-glu-rha-CO-CH2]^-$ ion at m/z 243. According to the literature, F10 was deduced as dihydroxy-methoxy-flavonone-O-rutinoside (39).

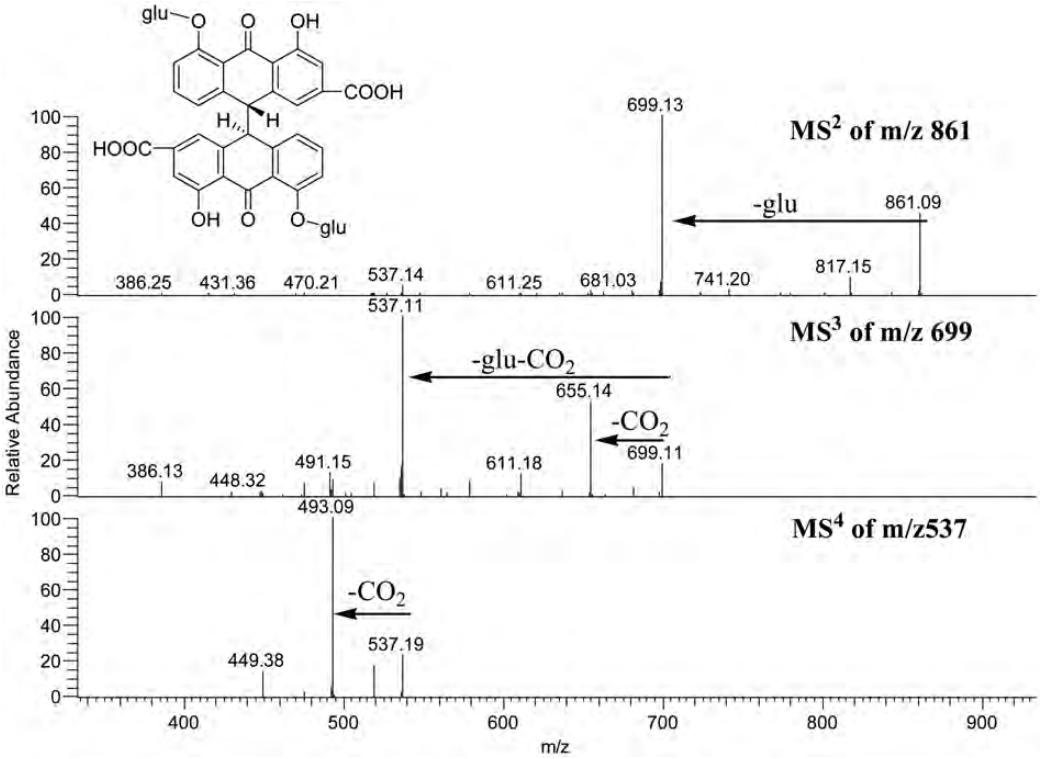

Figure 7. ESI-MS^n spectra of sennoside B.

ESI–MS-MS analysis of anthraquinones

In total, eight anthraquinones were isolated from XCQD as references consisting of six aglycones, one glycoside and sennoside B.

In the MS-MS spectrum of chrysophanol (MW = 254), a product ion at m/z 225 was obtained from its $[M\text{-}H]^-$ ion. The neutral loss of 28 Da was caused by the cleavage of CO from C-10. The other dominant peak at m/z 210 was formed by the drop of CO and CH_3 together. The fragment at m/z 182 in the MS^3 experiment indicated continued loss of CO from the other ketone. Emodin (MW = 270) and aloe-emodin (MW = 270) were two isomers with the same $[M\text{-}H]^-$ ion at m/z 269. Emodin revealed an $[M\text{-}H\text{-}CO]^-$ ion at m/z 241 and an $[M\text{-}H\text{-}CO_2]^-$ ion at m/z 225 in the MS-MS spectrum. However, $[M\text{-}H\text{-}CHO]^-$ ion at m/z 240 was considered to be the characteristic ion of aloe-emodin. MS^3 spectrum of m/z 240 yielded the fragment at m/z 211, which was attributed as the successive loss of the CHO group. Meanwhile, physcion (MW = 284) and rhein (MW = 284) were the other two isomers. Physcion yielded the $[M\text{-}H\text{-}15Da]^-$ ion in the MS-MS spectra, which was attributed to the loss of the methyl group. The further loss of CO from this obtained ion produced an $[M\text{-}H\text{-}CH3\text{-}CO]^-$ ion at m/z 240. Additionally, a series of even-numbered ions seemed to be the characteristic ions of physcion (15). As a comparison, rhein showed an $[M\text{-}H\text{-}C2H2]^-$ ion at m/z 257 and an $[M\text{-}H\text{-}CO2]^-$ ion at m/z 239 in the MS–MS spectrum.

In addition, 2-carboxy-3,8-dihydroxy-1-methylanthraquinone revealed an $[M\text{-}H]^-$ ion at m/z 297 in the full scan mass spectrum. The $[M\text{-}H\text{-}CO2]^-$ ion at m/z 253 was found to be the base peak in the MS-MS spectrum. Similar to the cleavage of chrysophanl, its MS^3 spectrum yielded a product ion at m/z 225.

Apart from free anthraquinones, emodin-8-O-glucoside (MW = 432) was also isolated from XCQD, which was the representative anthraquinone glycoside in rhubarb. An $[M\text{-}H\text{-}120Da]^-$ ion at m/z 311 was found to be the cleavage of glucose in the MS-MS spectrum. The aglycone ion at m/z 269 was shown to be the base peak. Identical to the fragmentation of emodin, the aglycone ion also yielded special ions at m/z 241 and 225 in the MS^3 spectrum.

In addition, as the typical compound of dianthrones, sennoside B (MW = 862) was detected in XCQD. In the MS-MS spectrum, sennoside B showed an $[M\text{-}H\text{-}glu]^-$ ion at m/z 699 as the base peak, and an $[M\text{-}H\text{-}CO2]^-$ ion at m/z 817 and an $[M\text{-}H\text{-}glu\text{-}glu]^-$ ion at m/z 537 were observed as the moderate peaks. Meanwhile, two low abundance peaks at m/z 741 and 579 were shown in the MS-MS spectrum, which was gradually produced by the elimination of glucosyl residue. Except for the base peak at m/z 537, the $[M\text{-}H\text{-}glu\text{-}CO2]^-$ ion at m/z 655 and the $[M\text{-}H\text{-}glu\text{-}120Da]^-$ ion at m/z 579 were significant in the MS^3 spectrum of $[M\text{-}H\text{-}glu]^-$ ion at m/z 699 (Figure 7).

Identification of anthraquinones

As the representative compounds from rhubarb, 31 anthraquinones were detected in the present study (Table IV). By comparison with references, six free anthraquinones were detected, including 2-carboxyl-3,8-dihydroxyl-1-methylanthraquinone (A21), aloe-emodin (A27), rhein (A28), emodin (A29), chrysophanol (A30) and physcion (A31).

Table IV
HPLC–ESI-MS^n Data Identification of Anthraquinones in XCQD*

Number	Name	T_R (min)	$[M-H]^-$ (*m/z*)	MS-MS (*m/z*)
A1	Chrysophanol-sinapoyl	28.89	459	MS^2 [459]: 415, 295, **253** MS^3 [459 → 253]: 253, 239, **225**, 166
A2	2-Carboxyl-3,8-dyhydroxyl-1-methylanthraquinone-glu	36.11	459	MS^2 [459]: **297** MS^3 [459 → 297]: 279, 261, **253**, 235, 209, 191, 176, 165
A3	Aloe-emodin-sinapoyl	39.74	475	MS^2 [475]: 431, 311, 283, **269** MS^3 [475 → 269]: **269,** 240, 201
A4	Chrysophanol-sinapoyl	43.38	459	MS^2 [459]: 295, 267, **253** MS^3 [459 → 253]: **253**, 198
A5	Sennoside	49.26	847	MS^2 [847]: 803, **685**, 684, 667, 641, 640, 523, 479, 386 MS^3 [847 → 685]: 668, 641, 623, 523, 505, 479, 462, 449, **386,** 370, 225
A6†	Sennoside B	51.34	861	MS^2 [861]: 817, **699,** 698, 655, 537 MS^3 [861 → 699]: 655, 654, **537**, 535, 493 MS^4 [861 → 699 → 537]: 519, **493,** 449, 224
A7	Edomin-O-glu-rha	51.81	577	MS^2 [577]: **269** MS^3 [577 → 269]: **269**, 224, 201, 200, 196, 181
A8	Hydroxide-rhein-O-rha-glu	53.34	607	MS^2 [607]: **299**, 284 MS^3 [607 → 299]: **284**
A9	Sennoside	55.54	861	MS^2 [861]: 817, **699**, 698, 655, 537 MS^3 [861 → 699]: 655, **537,** 536, 535, 519, 493, 492 MS^4 [861 → 699 → 537]: 519, 494, **492** MS^5 [861 → 699 → 537 → 492]: **447**
A10	Sennoside	56.39	861	MS^2 [861]: 817, **699**, 698, 655, 654, 611, 537 MS^3 [861 → 699]: 681, 655, 654, 593, 579, 549, **537**, 536, 535, 493, 492, 475, 387,
A11	Sennoside	56.63	847	MS^2 [847]: 803, **685**, 684, 667, 641, 640, 523, 479, 386 MS^3 [847 → 685]: 668, 641, 640, 523, 479, 462, **386**, 225, 224 MS^4 [847 → 685 → 386]: **224**
A12	Hydroxide-rhein-O-rha-glu	57.09	607	MS^2 [607]: 341, **299**, 284 MS^3 [607 → 299]: **284**
A13	Physcion-O-glu(OAc)	59.22	487	MS^2 [487]: 283, 269, 263, **239** MS^3 [487 → 239]: **211**
A14	Edomin-O-glu	59.50	431	MS^2 [431]: **269** MS^3 [431 → 269]: 269, 241, **225**, 210, 183
A15	Sennoside	61.91	861	MS^2 [861]: 817, **699**, 698, 697, 655, 537 MS^3 [861 → 699]: 655, **537**, 536, 493, 386 MS^4 [861 → 699 → 537]: 519, **493**, 492, 450, 224
A16	Chrysophanol-8-O-glu	64.48	415	MS^2 [415]: 325, 295, 277, 267, **253**, 237 MS^3 [415 → 253]: 226, **225**
A17	Carboxylation–methyl-dianthrone-O-glu-glu	65.03	831	MS^2 [831]: **669,** 668, 651, 624, 386 MS^3 [831 → 669]: 625, 580, 507, 506, 464, 463, 461, 446, **386**, 268 MS^4 [831 → 669 → 386]: **224**
A18†	Emodin-8-O-glu	65.52	431	MS^2 [431]: 311, 293, **269**, 268 MS^3 [431 → 269]: 269, 241, **225** MS^4 [431 → 269 → 225]: **210**, 182
A19	Emodin-O-(6′-O-malonyl)-glu	66.01	517	MS^2 [517]: **473** MS^3 [517 → 473]: 311, **269** MS^4 [517 → 473 → 269]: 269, 241, **225**, 224 MS^5 [517 → 473 → 269 → 225]: 198
A20	Aloe-emodin-O-glu(OAc)	66.84	473	MS^2 [473]: **268** MS^3 [473 → 268]: 268, **267**
A21†	2-Carboxyl-3,8-dihydroxyl-1-methylanthraquinone	67.20	297	MS^2 [297]: **253** MS^3 [297 → 253]: **253**, 238, 225
A22	11-O-Acetyl-aloe-emodin-O-glu-xyl	69.34	605	MS^2 [605]: **311**, 283, 269, 268 MS^3 [605 → 311]: 283, 269, **268** MS^4 [605 → 311 → 268]: **240**
A23	Emodin-O-glu	69.54	431	MS^2 [431]: **268** MS^3 [431 → 268]: **268,** 267, 240, 226, 224
A24	Dicarboxylation-dianthrone-O-glu-glu(OAC)	70.29	903	MS^2 [903]: **859**, 697, 458 MS^3 [903 → 859]: 697, **458**, 441, 416 MS^4 [903 → 859 → 458]: 267, **255**, 254
A25	Feruloyl-aloe-emodin-methoyl-cinnamoyl ester	71.65	605	MS^2 [605]: **561** MS^3 [605 → 561]: 413, 269, **268,** 240 MS^4 [605 → 561 → 268]: **240** MS^5 [605 → 561 → 268 → 240]: **212,** 211
A26	Acetyl-chrysophanol-O-glu-xyl	72.17	589	MS^2 [589]:457, 295, **253**, 252 MS^3 [589 → 253]: 225, **224**
A27†	Aloe-emodin	74.05	269	MS^2 [269]:269, **240** MS^3 [269 → 240]:**211**
A28†	Rhein	75.61	283	MS^2 [283]: **257,** 241, 239 MS^3 [283 → 257]: 257, 241, **239** MS^4 [283 → 257 → 239]: 257, 229, **212**, 195
A29†	Emodin	82.33	269	MS^2 [269]: 241, **225**, 211 MS^3 [269 → 225]: **197**
A30†	Chrysophanol	85.29	253	MS^2 [253]: **225**, 210 MS^3 [253 → 225]: **182**

(*continued*)

Table IV Continued

Number	Name	T_R (min)	$[M-H]^-$ (m/z)	MS-MS (m/z)
A31†	Physcion	85.74	283	MS^2 [283]: 268, **240**

*Note: Bold characters indicate the base peaks in MS^n spectra.
†Structures confirmed by comparison with reference standards.

A18 was definitely identified as emodin-8-O-glucoside (MW = 432, t_R = 65.52 min) by comparison with the reference. A14 (MW = 432, t_R = 59.50 min) and A23 (MW= 432, tR = 69.54 min) were clearly detected as two isomers of A18. Their MS-MS fragmentations presented $[M-H-glu]^-$ and $[M-H-glu]^-$ ions at m/z 269 and 268, respectively. The presence of a radical ion in A24 was caused by the different substitution positions of glucose and the different negative center on the aglycone ions. By referring to the literature, A14 and A23 were assigned as emodin-1-O-glucoside and emodin-5-O-glucoside, respectively (40).

A16 (MW = 416, t_R = 64.48 min) showed an $[M-H]^-$ ion at m/z 415 in the negative ion scan mode. Its MS-MS spectrum clearly revealed the base peak at m/z 253. In addition, the $[M-H-120Da]^-$ ion at m/z 295 was obvious. Combined with the ion obtained at m/z 225 in the MS^3 experiment, A16 was deduced to be chrysophanol-8-O-glucoside (41).

Apart from monoglycosides, anthraquinone with two sugars were also detected in XCQD. A26 (MW = 590, t_R = 72.17 min) presented a base peak at m/z 253 in the MS-MS spectrum, elucidating the existence of chrysophanol aglycone. The moderate peak at m/z 295 was also found, which originated from the cleavage of glycoside. In all, the neutral loss of 336 from the $[M-H]^-$ ion was attributed to be the cleavage together of glu(OAc) and xylose groups. Meanwhile, the $[M-H-xyl]^-$ ion at m/z 457 was detected as a low abundance peak. Thus, A26 was deduced as chrysophanol-O-glu(OAc)-xyl.

In the MS-MS spectrum of A3 (MW = 476, t_R = 39.74 min), the $[M-H-44Da]^-$ ion at m/z 431 was found to be the predominant peak. This obtained ion was subjected to MS^3 analysis to generate an aglycone ion at m/z 269 as the base peak. The successive losses of 44 Da and 162 Da were in accordance with the sinapoyl group. Meanwhile, the characteristic ion at m/z 240 was found in the low molecular region, which was identical to aloe-edomin. Thus, A3 was assigned as aloe-edomin-sinapoyl.

A19 (MW = 518, t_R = 66.01 min) showed a frequent neutral loss of 44 Da and 204 Da in the MS-MS and MS^3 spectra, which was considered to be the diagnostic fragmentation of glucose-malonate. The characteristic ions of emodin at m/z 241 and 225 were found in further MS^4 experiments. Based on the references, A19 was deduced as emodin 8-O-(6′-O-malonyl)-glucoside (42).

A20 (MW = 474, t_R = 66.84 min) gave an $[M-H]^-$ ion at m/z 473 in the full scan mass spectrum. Its MS-MS spectrum showed an $[M-H-204Da]^-$ ion at 268 as the base peak. The neutral loss of 204 Da was attributed as the loss of glu(OAc). In the further MS^3 spectrum of m/z 268, the characteristic ion at m/z 240 indicated that the aglycone of A20 was aloe-emodin. Thus, this compound was identified as aloe-emodin-O-glu(OAc).

A22 and A26 were additionally detected as two acetylated anthraquinone glycosides. In the MS-MS spectrum of A22 (MW = 606, t_R = 69.34 min), $[M-H-glu-xyl]^-$ ion at m/z 311 was detected as the base peak. The further MS^3 experiments of this ion exhibited the $[M-H-glu-xyl-acetyl]^-$ ion at m/z 268 as the base peak. In addition, two small peaks at m/z 283 and 269 were found. In the MS^4 spectrum of m/z 268, the characteristic ion of aloe-emodin at m/z 240 was detected. Thus, the aglycone ion at m/z 311 of A22 was deduced as acetyl-aloe-emodin. According to the literature, the acetyl group should attach at the C-11 position (43). Therefore, A22 was identified as 11-O-acetyl-aloe-emodin-glu-xyl.

Similar to A22, A26 (MW = 589, t_R = 72.17 min) presented $[M-H-glu-xyl]^-$ as the significant ion at m/z 295 in the MS-MS spectrum. The $[M-H-glu-xyl-acetyl]^-$ ion at m/z 253 was shown as the base peak. With the further MS^3 fragments at m/z 224 and 225 taken into consideration, the aglycone of A26 was deduced as acetyl-chrysophanol. Therefore, A26 was attributed as acetyl-chrysophanol-glu-xyl.

However, as the isomer of A22, A25 (MW = 606, t_R = 71.65 min) presented different ESI-MS fragmentations. In the MS-MS spectrum, an $[M-H-CO_2]^-$ ion at m/z 561 was found as the base peak. The MS^3 spectrum exhibited the $[M-H-feruloyl]^-$ ion at m/z 413 as moderate peak and the $[M-H-feruloyl-methoxyl-cinnamoyl]^-$ ion at m/z 268 as the base peak. In the MS^4 spectrum of m/z 268, the characteristic ion of aloe-emodin at m/z 240 was clearly observed. Two positions of aloe-emodin were substituted. Methoxyl-cinnamoyl contacts with aloe-emodin by ester bond. Thus, A25 was tentatively deduced as feruloyl-aloe-emodin-methoxyl-cinnamoyl ester.

Rhein glycoside was also detected as A13 (MW = 488, t_R = 59.22 min) in XCQD. Its MS-MS spectrum gave the base peak at m/z 239. Meanwhile, an ion with natural loss of 204 Da at m/z 283 was presented as the moderate peak, which indicated the existence of glu(OAc). Further MS^3 analysis of m/z 239 also supported the existence of rhein aglycone. Therefore, A13 was characterized as rhein-8-O-glu (OAc) (13).

Additionally, as an important type of anthraquinone, six sennosides have been reported from rhubarb species (sennosides A–F) (44). In XCQD, XIC of m/z 847 gave A5 and A11 at t_R = 49.26 and 56.63 min, respectively. Almost the same fragmentations were presented in their MS^n spectra. The continuous neutral loss of glucosyl residue at m/z 685 and 543 were found in MS^2 and MS^3 spectra. Their structures were identified as sennodides C and D. Additionally, three isomers of sennodide B (A6, MW = 862, t_R = 51.34 min) were detected at 55.54, 56.39 and 61.91 min. It was very difficult to discriminate them only by their MS spectra. Sennoside A and its isomer should be included in these three compounds (13, 45).

ESI–MS-MS analysis of magnolol

Magnolol was observed at 86.97 min. The $[M\text{-}H]^-$ ion at m/z 265 was presented in the full mass scan spectrum. This obtained ion produced an $[M\text{-}H_2O\text{-}H]^-$ ion at m/z 247 as the base peak in the MS^2 spectrum. This ion was resulted from the dehydration of two phenolic hydroxyls. Meanwhile, the $[M\text{-}C_3H_5\text{-}H]^-$ peak at m/z 224 was observed, which was caused by the loss of the propylene branch (47, 48). Magnolol seemed to be the representative constituents from *Cortex Magnoliae Officinalis*. However, the content was very low. *Cortex Magnoliae Officinalis* primarily contributed its volatile components in the prescription.

Conclusions

In the present paper, an HPLC–ESI-IT-MS method was developed for chemical profile analysis of XCQD. In total, 26 tannins and their precursors, 13 flavanones, 31 anthraquinones and magnolol were identified or tentatively characterized by their MS fragmentations and chromatographic behavior. T10, T16, T24, T25, A2, A3, A4, A12, A17, A24, A25 and A26 were reported in this paper for the first time. Additionally, the ESI-MS fragmentation patterns of three flavanone glycosides (naringin, hesperidin and neohesperidin) were investigated. The mass spectra difference between hesperidin and neohesperidin was clarified. In this investigation, the contents of flavonones from *Fructus Aurantii Immaturus* presented relatively higher amounts than anthraquinones. This was identical to the determination results of XCQD (46). Therefore, it was suggested that flavanones and anthraquinones should be used together for the quality control of XCQD. The further synergistic effect study of tannins, flavanones and anthraquinone should be conducted.

Acknowledgments

This work was supported by program for National Key Technology R&D Project (No. 2008BAI51B02). The assistance of Prof. Xi-Rong He in the identification of herb medicines is gratefully acknowledged.

References

1. Tseng, S.H., Chien, T.Y., Tzeng, C.F., Lin, Y.H., Wu, C.H., Wang, C.C.; Prevention of hepatic oxidative injury by Xiao-Chen-Chi-Tang in mice; *Journal of Ethnopharmacology*, (2007); 111: 232–239.
2. Wu, Z., Wang, Q.; The clinical use of Xiao-Cheng-Qi Decoction; *Shanxi Traditional Chinese Medicine Journal*, (1984); 5: 25–26.
3. Qin, Y., Wang, J., Kong, W., Zhao, Y., Yang, H., Dai, C., *et al.*; The diarrheogenic and antidiarrhoeal bidirectional effects of rhubarb and its potential mechanism; *Journal of Ethnopharmacology*, (2010); 133: 1096–1102.
4. Yagi, T., Yamauchi, K.; Shojoki-to (Xiao-Cheng-Qi-Tang), immature orange, magnolia bark, rhubarb, rat, colonic circular muscle motility; *Journal of Traditional Medicine*, (2002); 19: 98–102.
5. Dechang, C., Jiandong, Y., Bingwen, J.; Effect of rhubarb on permeability changes in intestinal mucosa and capillary; *Chinese Critical Care Medicine*, (1997); 9: 385–387.
6. Tseng, S.H., Lee, H.H., Chen, L.G., Wu, C.H., Wang, C.C.; Effects of three purgative decoctions on inflammatory mediators; *Journal of Ethnopharmacology*, (2006); 105: 118–124.
7. Tseng, S.H., Chien, T.Y., Chen, J.R., Lin, I.H., Wang, C.C.; Hypolipidemic effects of three purgative decoctions; *Evidence-Based Complementary and Alternative Medicine*, (2011); 249–254.
8. Jia, C.H., Wang, Y.Y., Huang, Q.F., Lu, Z.L., Q.G., W.; Review of research on clinical applications of combined prescriptions; *Journal of Beijing University of Traditional Chinese Medicine*, (2005); 28: 9–33.
9. Yu, J., Yu, Z.H.; The clinical observation for stroke with hyperlipidemia treated by Xiao-Cheng-Qi Decoction; *Journal of Changchun College of Traditional Chinese Medicine*, (1999); 15: 12.
10. Sheu, S.J., Lu, C.F.; Determination of eight constituents of Hsiao-cheng-chi-tang by high-performance liquid chromatography; *Journal of Chromatography A*, (1995); 704: 518–523.
11. Fan, M., Wang, H., Li, X., Li, P., Bian, B.; Studies on chemical constituents and volatile oil of Xiaochengqi decoction; *Journal of Chinese Medicinal Materials*, (2008); 33: 1027–1031.
12. Hvattum, E., Ekeberg, D.; Study of the collision-induced radical cleavage of flavonoid glycosides using negative electrospray ionization tandem quadrupole mass spectrometry; *Journal of Mass Spectrometry*, (2003); 38: 43–49.
13. Ye, M., Han, J., Chen, H., Zheng, J., Guo, D.; Analysis of phenolic compounds in rhubarbs using liquid chromatography coupled with electrospray ionization mass spectrometry; *Journal of American Society for Mass Spectrometry*, (2007); 18: 82–91.
14. Qiang, J., Yang, B., Yan, M., Wei, P., Wei-wei, S.; Chemical constituents of *Fructus Aurantii* and *Fructus Aurantii Immaturus* by HPLC-ESI-MS; *Chinese Traditional Herb Drug*, (2005); 36: 169–172.
15. Dong, J., Wang, H., Wan, L., Hashi, Y., Chen, S.; Identification and determination of major constituents in *Polygonum cuspidatum Sieb.* et Zucc. by high performance liquid chromatography/electrospray ionization-ion trap-time-of-flight mass spectrometry; *Chinese Journal of Chromatography*, (2009); 27: 425–430.
16. Rubilar, M., Pinelo, M., Shene, C., Sineiro, J., Nuñez, M.J.; Separation and HPLC-MS identification of phenolic antioxidants from agricultural residues: Almond hulls and grape pomace; *Journal of Agricultural and Food Chemistry*, (2007); 55: 10101–10109.
17. Ding, M., Ni, W.; Separation of tannins in rhubarb and its analysis by high performance liquid chromatography-mass spectrometry; *Chinese Journal of Chromatography*, (2004); 22: 605–608.
18. Wang, Q., Chen, L., Tian, Y., Li, B., Sun, Q.H., Dong, J.X.; Chemical constituents of *Polygonum perfoliatum* L.; *Bulletin of the Academy of Military Medical Sciences*, (2009); 33: 254–256.
19. Jin, W., Wang, Y.F., Ge, R.L., Shi, H.M., Jia, C.Q., Tu, P.F.; Simultaneous analysis of multiple bioactive constituents in *Rheum tanguticum Maxim.* ex Balf. by high-performance liquid chromatography coupled to tandem mass spectrometry; *Rapid Communications in Mass Spectrometry*, (2007); 21: 2351–2360.
20. Li, S.L., Song, J.Z., Qiao, C.F., Zhou, Y., Xu, H.X.; UPLC-PDA-TOFMS based chemical profiling approach to rapidly evaluate chemical consistency between traditional and dispensing granule decoctions of traditional medicine combinatorial formulae; *Journal of Pharmaceutical and Biomedical Analysis*, (2010); 52: 468–478.
21. Jiang, Z.H., Hirose, Y., Iwata, H., Sakamoto, S., Tanaka, T., Kouno, I.; Caffeoyl, coumaroyl, galloyl, and hexahydroxydiphenoyl glucoses from *Balanophora japonica*; *Chemical and Pharmaceutical Bulletin*, (2001); 49: 887–892.
22. Panthama, N., Kanokmedhakul, S., Kanokmedhakul, K.; Galloyl and hexahydroxydiphenoyl esters of phenylpropanoid glucosides, phenylpropanoids and phenylpropanoid glucosides from rhizome of *Balanophora fungosa*; *Chemical and Pharmaceutical Bulletin*, (2009); 57: 1352–1355.
23. Wang, W., Zeng, S.F., Yang, C.R., Zhang, Y.J.; A new hydrolyzable tannin from *Balanophora harlandii* with radical-scavenging activity; *Helvetica Chimica Acta*, (2009); 92: 1817–1822.
24. Ossipov, V., Loponen, J., Ossipova, S., Haukioja, E., Pihlaja, K.; Gallotannins of birch *Betula pubescens* leaves: HLPC separation and quantification; *Biochemical Systematics and Ecology*, (1997); 25: 493–504.

25. Song, F., Wu, F., Zhong, Z.; Determination of (+)-catechin and (−)-epicatechin and berberine hydrochloride in Wangying capsule by RP-HPLC; *Chinese Traditional Patent Medicine*, (2006); 28: 806–810.
26. Nonaka, G., Ezaki, E., Hayashi, K., Nishioka, I.; Flavonol glucosides from rhubarb and *Rhaphiolepis umbellate*; *Phytochemistry*, (1983); 22: 1659–1661.
27. Fossen, T., Anderson, O.M., Ovstedal, D.A.G.O., Pedersen, A.T., Raknes, A.S.E.; Characteristic anthocyanin pattern from onions and other *Allium* spp; *Journal of Food Science*, (1996); 61: 703–706.
28. Mayer, W., Schultz, G., Wrede, S., Schilling, G.; 2-O-Cinnamoyl-1-O-galloyl-β-D-glucopyranose aus Rhizoma rhei; *European Journal of Organic Chemistry*, (1975); 1975: 946–952.
29. Shi, P., He, Q., Song, Y., Qu, H., Cheng, Y.; Characterization and identification of isomeric flavonoid O-diglycosides from genus Citrus in negative electrospray ionization by ion trap mass spectrometry and time-of-flight mass spectrometry; *Analytica Chimica Acta*, (2007); 598: 110–118.
30. Hasan, A., Tahir, M.N.; Flavonoids from the leaves of *Impatiens bicolor*; *Turkish Journal of Chemistry*, (2005); 29: 65–70.
31. Djoukeng, J.D., Arbona, V., Argamasilla, R., Gomez-Cadenas, A.; Flavonoid profiling in leaves of Citrus genotypes under different environmental situations; *Journal of Agricultural and Food Chemistry*, (2008); 56: 11087–11097.
32. Xu, F., Liu, Y., Song, R., Dong, H., Zhang, Z.; Constituents of Da-Cheng-Qi decoction and its parent herbal medicines determined by LC-MS/MS; *Natural Product Communications*, (2010); 5: 789–794.
33. Ma, C., Gao, W., Gao, Y., Man, S., Huang, L., Liu, C.; Identification of chemical constituents in extracts and rat plasma from *Fructus Aurantii* by UPLC-PDA-Q-TOF/MS; *Phytochemical Analysis*, (2010); 22: 112–118.
34. Qiao, X., Ye, M., Liang, Y.H., Yang, W.Z., Guo, D.A.; Retention behaviors of natural products in reversed-phase liquid chromatography using mobile phase comprising methanol, acetonitrile and water; *Journal of Separation Science*, (2011); 34: 169–175.
35. Ablajan, K., Abliz, Z., Shang, X.Y., He, J.M., Zhang, R.P., Shi, J.G.; Structural characterization of flavonol 3, 7-di-O-glycosides and determination of the glycosylation position by using negative ion electrospray ionization tandem mass spectrometry; *Journal of Mass Spectrometry*, (2006); 41: 352–360.
36. Nakagawa, H., Takaishi, Y., Tanaka, N., Tsuchiya, K., Shibata, H., Higuti, T.; Chemical constituents from the peels of *Citrus sudachi*; *Journal of Natural Product*, (2006); 69: 1177–1179.
37. Xu, X., Jiang, J., Liang, Y., Yi, L., Cheng, J.; Chemical fingerprint analysis for quality control of *Fructus Aurantii Immaturus* based on HPLC-DAD combined with chemometric methods; *Analytical Methods*, (2010); 2: 2002–2010.
38. Berhow, M.A., Bennett, R.D., Kanes, K., Poling, S.M., Vandercook, C.E.; A malonic acid ester derivative of naringin in grapefruit; *Phytochemistry*, (1991); 30: 4198–4200.
39. Kawaii, S., Tomono, Y., Katase, E., Ogawa, K., Yano, M., Koizumi, M., *et al.*; Quantitative study of flavonoids in leaves of citrus plants; *Journal of Agricultural and Food Chemistry*, (2000); 48: 3865–3871.
40. Zhang, C., Li, L., Xiao, Y.Q., Tian, G.F., Chen, D.D., Wang, Y., *et al.*; Two new anthraquinone glycosides from the roots of *Rheum palmatum*; *Journal of Asian Natural Products Research*, (2010); 12: 1026–1032.
41. Okabe, H., Matsuo, K., Nishioka, I.; Studies on rhubarb (*Rhei rhizoma*). II. Anthraquinone glycosides; *Chemical and Pharmaceutical Bulletin*, (1973); 21: 1254–1260.
42. Püssa, T., Raudsepp, P., Kuzina, K., Raal, A.; Polyphenolic composition of roots and petioles of *Rheum rhaponticum* L; *Phytochemical Analysis*, (2009); 20: 98–103.
43. Fu, W., Tan, C., Meng, X., Lu, L., Jiang, S., Zhu, D.; Isolation and identification of the chemical constituents from root of *Actinidia deliciosa*; *Chinese Journal of Medicinal Chemistry*, (2010); 20: 116–118.
44. Oshio, H., Imai, S., Fujioka, S., Sugawara, T., Miyamoto, M., Tsukui, M.; Investigation of Rhubarbs. III. New purgative constituents, sennosides E and F; *Chemical and Pharmaceutical Bulletin*, (1974); 22: 823–831.
45. Xu, F., Liu, Y., Song, R., Dong, H., Tian, Y., Zhang, Z.; Correlation of material base between Da-Cheng-Qi decoction and its principal drug rhubarb by LC-MS/MS; *Journal of China Pharmaceutical University*, (2008); 39: 136–141.
46. Liu, Y., Liu, X., Wang, Q.; Quality analysis of Da, Xiao-Chengqi Decoction produced in Taiwan; *Chinese Traditional Patent Medicine*, (2009); 31: 547–550.
47. Zeng, Z, Shen, M., Meng, S.; Applications of organic mass spectrometry to structure elucidation of osthole, magnolol, honokiol and houttuynium; *Chinese Journal of Organic Chemistry*, (2007); 27: 92–96.
48. Zeng, Z., Zhao, F., Meng, S.; Applications of organic mass spectrometry in structure elucidation of magnolol and honokiol; *Journal of Chinese Mass Spectrometry Society*, (2006); 27: 65–70.